Acta Materialia 99 (2015) 99–105

Contents lists available at ScienceDirect

Acta Materialia

journal homepage: www.elsevier.com/locate/actamat

Dislocation depinning from nano-sized irradiation defects in a bcc iron model

Julien Dérès, Laurent Proville *, Mihai-Cosmin Marinica

CEA, DEN, Service de Recherches de Métallurgie Physique, 91191 Gif sur Yvette, France

ARTICLE INFO

Article history:
Received 2 June 2015
Accepted 26 July 2015

Keywords:
Dislocation
Irradiation hardening
Atomic simulations
Iron based alloys

ABSTRACT

At the atomic level, irradiation hardening of a body-centered-cubic (bcc) crystal of iron is investigated through the study of a dislocation interaction with nano-sized obstacles of various types, i.e. nano-voids, dislocation loops with ⟨1 0 0⟩ and 1/2⟨1 1 1⟩ Burgers vectors, and C15 clusters. The dislocation pinning is common to every type of cluster excepted for loops with 1/2⟨1 1 1⟩ Burgers vector, the mobility of which allows them to glide along with dislocation, thence yielding a minor contribution to hardening. At bypassing of anchoring clusters, the dislocation is found to yield a pair of jogs throughout a process of local climb due to the absorption of vacancies or of self-interstitial atoms that form the clusters. In order to rationalize our simulation results, we have employed an analytical theory proposed by Bacon and Scattergood (1982) which is extended phenomenologically to treat all anchoring defects, including C15 clusters and ⟨1 0 0⟩ loops. For small clusters, below 17 elementary defects, the simulation results deviate from the analytical predictions, and the different types of cluster correspond to different pinning strengths amongst those of C15 clusters appear to be the largest, emphasizing a possible important contribution to irradiation hardening in iron based alloys.

1. Introduction

Nuclear reactor engineering is demanding materials with high resistance to elevated temperatures and irradiation doses, some requirements that have long been recognized into the bcc iron based alloys [1]. In the long term use of these materials [2], the motion of dislocations is obstructed by nano-sized clusters made of vacancies or self-interstitial atoms (SIA), i.e. the elementary point like defects produced in the crystal along the collisions between its atoms with incident neutrons and the subsequent displacement cascades. The accumulation of obstacles makes the mobility of dislocations more and more limited and consequently increases the fragility of the material, which contributes to explain qualitatively why the ductile to brittle transition (DBT) is displaced toward higher temperatures with irradiation doses [3].

Regarding the variety of obstacles, iron has a specific feature compared to all other bcc metals. The Burgers vectors of dislocation loops observed by transmission electron microscopy (TEM) are either 1/2⟨1 1 1⟩ or ⟨1 0 0⟩, depending on temperature [4,5], whereas in other bcc metals, most of loops have 1/2⟨1 1 1⟩ Burgers vector. For sizes between single elementary point like defects and nanometric clusters, the TEM observations have not sufficient precision to conclude but using the predictive power of modern electronic structure calculations, a new class of interstitial clusters has been found in bcc iron [6,7]. With a three dimensional structure by contrast with the conventional two dimensional dislocation loops, these clusters have a structure which corresponds to the C15 Laves phase. In iron, these C15 aggregates are highly stable, immobile and can form spontaneously under irradiation, growing through the capture of single self-interstitial atoms. The density, kinetics and the growth of these obstacles are still under debate [8–10] as well as their involvement with the microstructure. The present study allows us to shed light onto the C15 clusters interaction with dislocations by comparison with the more conventional obstacles observed in different experimental works such as voids and dislocation loops with 1/2⟨1 1 1⟩ or ⟨1 0 0⟩ Burgers vectors [2,11–13].

Computer simulations to investigate the interaction of dislocations with different obstacles have first been performed through the discrete dislocation model. The latter emerged from the pioneering work of Foreman [14] and Bacon [15] in the seventies, where dislocations were described as connected segments within line tension approximation. These works can be considered as the ancestors of the discrete dislocation dynamics (DDD) models [16,17] that are now highly efficient to model many-dislocation

* Corresponding author.
E-mail address: laurent.proville@cea.fr (L. Proville).

http://dx.doi.org/10.1016/j.actamat.2015.07.067
1359-6454/

dynamics at microscopic scale, inside a grain of matter. On the basis of their computational results, Bacon et al. (BKS) [18] established an analytical model where the critical resolved shear stress (CRSS) required for an edge dislocation to bypass a regular array of inclusions can be written as

$$\tau_{BKS} = \frac{Gb}{2\pi L}\left[\ln\left(\frac{2rL}{2r+L}\right) + B\right], \quad (1)$$

where G is the effective shear modulus, b is the Burgers vector, r is the radius of the precipitate, L is the distance that separates the surfaces of inclusions and B is an adjustable parameter. It has been established that the CRSS associated to cavities is correlated to Eq. (1) with $B = 1.52$ while for impenetrable obstacles $B = 0.7$, as determined from dawning DDD computations [15,19].

Based on the embedded atom method (EAM) [20,21] the interaction of dislocations with voids [22–25], stacking fault tetrahedra [26] or with interstitial loops [27–29] were studied at the atomic scale through molecular dynamics (MD) simulations. However, because of the computational load of such a method, it cannot serve to model materials within realistic dimensions and realistic deformation rates, compelling to take up the challenge of a multi-scale approach where the information captured throughout atomic scale simulations must be conveyed to larger scales. This task can be achieved either by adjusting DDD parameters to reproduce MD results [30,31] or by validating analytical theory as BKS that can be extrapolated to larger scales [23]. For the present study, we have chosen the second option. We employ an EAM well adapted for irradiation point defects in bcc iron [32], in order to realize the simulations for dislocation interaction with the different types of obstacles potentially yielded by irradiation [6,7]. We confirm that Eq. (1) with $B = 1.52$ predicts satisfactorily the CRSS associated with voids above a certain size, with no more adjusted parameter. Noteworthily the very same equation is also shown to be well adapted to predict the CRSS associated with clusters of SIA, i.e. dislocation loops with $\langle 1\,0\,0\rangle$ Burgers vectors, as well as for C15 clusters. The rather good agreement between theory and simulations holds for clusters of sizes larger than a certain number of elementary defects, i.e. down to 17 SIA for loops and C15 clusters and down to 17 vacancies for voids, which corresponds to a radius of 5 Å, approximately. Below this threshold the C15 clusters are found to be the strongest obstacles to the passage of dislocations. The dislocation loops with $1/2\langle 1\,1\,1\rangle$ Burgers vectors are found to present a much smaller resistance to dislocation passage, as their intrinsic mobility allows them to glide along with dislocations.

The present paper is organized as follows. First, in Section 2 the simulations for the depinning process of dislocations are described and the CRSS associated with the different types of obstacle is computed. The results are analyzed in Section 3 while our conclusions are drawn in Section 4.

2. Simulations of dislocation depinning

Our study is limited to the case of edge dislocations as their mobility is characterized by small Peierls barriers, in contrast to screw ones, the glide of which implies the propagation of kinks and a particular theoretical treatment [33,34] to determine correctly the stress threshold at which the glide process occurs. The depinning threshold of an edge dislocation from a distribution of nano-sized obstacles in a bcc iron single crystal is computed through the EAM named after M07 in Ref. [32]. The main interest of using this inter-atomic potential is to reproduce well the relative stability of defect clusters yielded by irradiation, in comparison to ab initio computations [6]. The variability of our results according to the atomic-scale model is discussed later on. To study the dislocation depinning, the simulation cell was set up with the following crystal geometry: the $[1\,1\,\bar{2}]$ direction in X, the $[1\,1\,1]$ direction in Y, and the $[1\,\bar{1}\,0]$ direction in Z. The details for the construction of the simulation cell, for the shear stress application and for the introduction of the dislocation have been detailed in earlier works [21,27,35–37]. The dislocation's Burgers vector is $b = \frac{a_0}{2}[1\,1\,1]$, which corresponds to the glide direction for the edge dislocation. Here, a_0 represents the lattice parameter of the perfect bcc lattice of α-Fe. A single cluster made of either vacancies or SIA's is introduced at a position as far as possible from the dislocation and an energy minimization procedure is applied to find the ground state of the system. The periodic boundary conditions along the direction X, i.e. the dislocation line, result in a periodic row of obstacles with spacing corresponding to the dimension of the simulation cell in the X direction. The applied stress is incremented gradually by 5 MPa and a relaxation procedure is applied after each increment, which allows us to determine the CRSS in quasi-static conditions by contrast with some previous studies where the deformation rate was imposed [23–25]. The dimensions of the simulation cell perpendicular to the glide plane and in the glide direction were chosen such that the depinning threshold has a negligible dependency with respect to these dimensions. The spherical obstacles as voids or C15 clusters are introduced in the simulation cell such that the dislocation glide plane cuts the obstacle through its largest dimensions. It has been shown [38] that the pinning strength remains significant provided that the dislocation glide plane intersects the obstacle boundary surface, although it decreases gradually with the distance of the glide plane to the largest section of a void. The trend is the same for the different types of obstacle, even for planar ones such as loops the habit plane of which intersects the dislocation glide plane.

In the case of loops with a $\{\bar{1}\,0\,1\}$ habit plane, i.e. the same as the dislocation glide plane, the range of the interaction is limited to the nearest planes to the glide plane while for other obstacles the interaction expands over the size of the obstacles. The probability for a dislocation to cross a loop with a $\{\bar{1}\,0\,1\}$ habit plane is therefor independent of the loop size by contrast with other obstacles. As a consequence, we can expect a minor role for such obstacles in the statistics of dislocation pinning. For that reason, we consider only the loops that cross the dislocation glide plane. The loops are introduced in the simulation cell such that their intersection with the dislocation glide plane corresponds to their diameters.

In agreement with earlier studies [25,38,39], the dislocation is attracted by voids and enters in them creating surface steps, and finally breaks away when the applied stress reaches the CRSS. The edge dislocation climbs by absorbing few vacancies from the void during the interaction. The number of absorbed vacancies depends on the size of the obstacle but the absorption sites correspond to the region of compression of the edge dislocation. In Fig. 1(a), we have reported a sequence of images from our simulations, which confirms the sketch of the interaction between the dislocation and voids. As shown in Fig. 1(b) for C15 clusters and in Fig. 1(c) for loops with $\langle 1\,0\,0\rangle$ Burgers vector, our simulations show that the depinning process for obstacles made of SIA's is the same as for voids, but the climb is inverted because of the nature of the defects (compare insets with jogs in Fig. 1(a) and in Fig. 1(b and c)). The interstitial atoms are preferably absorbed in the region of tensile stress around the dislocation core. In the case of $\langle 1\,0\,0\rangle$ loops, in agreement with the work from Terentyev et al. [28] we have observed that the reaction with the dislocation depends on the size of the loop. After bypassing small loops, a part of the loop is left behind the gliding dislocation whereas for loops above a certain critical size (comprised between 49 and 97) the bypassing leads to the total absorption of the loops and to the formation of large jogs on the dislocation line. The previous works

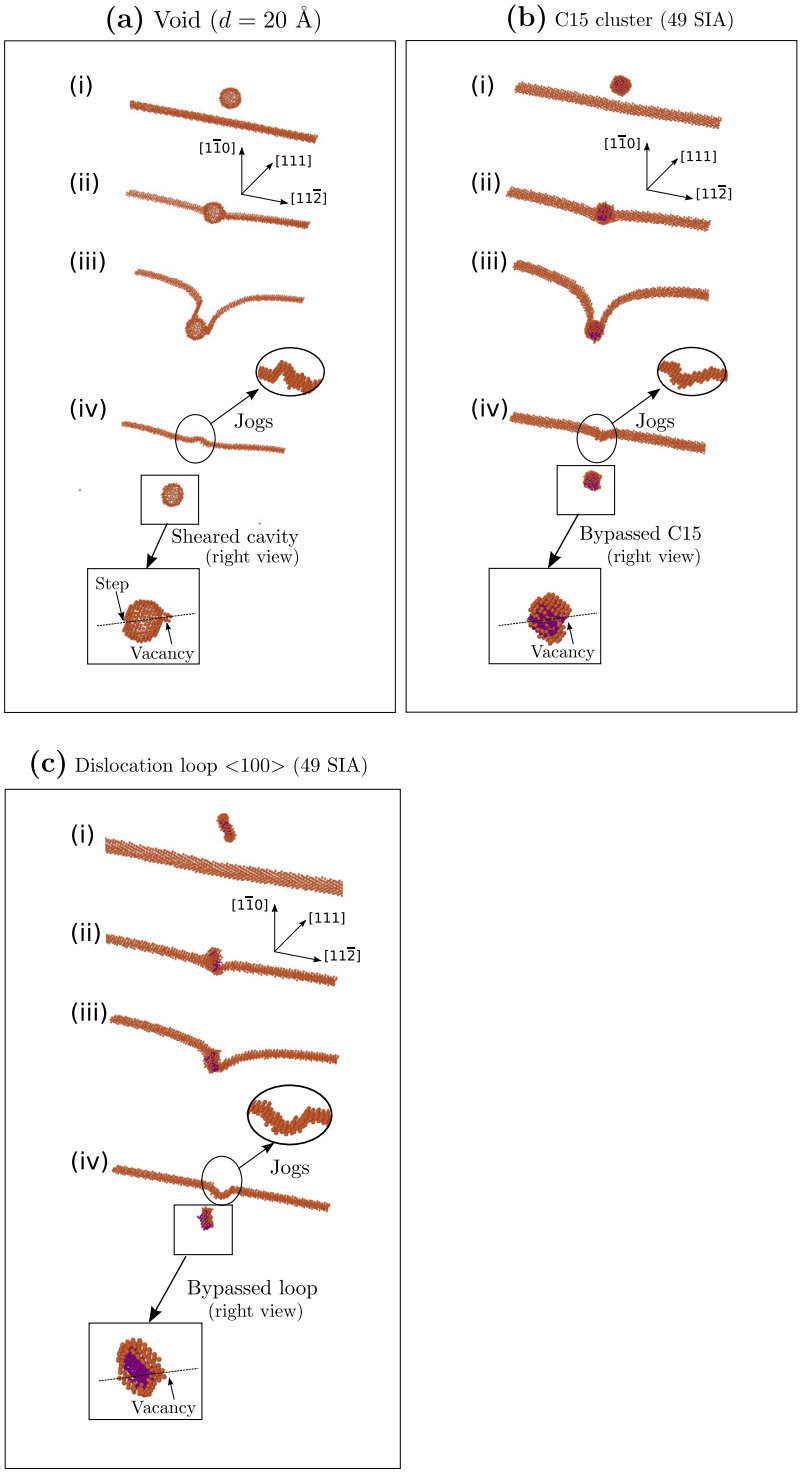

Fig. 1. (a–c) Snapshots of the crossing process for an edge dislocation in interaction with a periodic row of nano-obstacles, separated by L = 21 nm in $X = [1\ 1\ \bar{2}]$ direction. The obstacles are made of (a) voids with 10 Å diameter, (b) C15 nano-cluster of 49 SIA's and (c) dislocation loop with ⟨1 0 0⟩ Burgers vector, of 49 SIA and with orientation $v1$ (see text). The different stages of the simulations are represented: (i) before bypassing at a stress smaller than the Peierls stress (≈25 MPa), (ii) the dislocation is anchored on the obstacle at a stress of the order of the Peierls stress, (iii) at the critical resolved shear stress, the dislocation reaches a profile with a maximal bend, (iv) after bypassing. The SIA's added in the bcc crystal are colored in violet and other atoms are colored in orange if their first neighbor cell does not fit the bcc local symmetry. (For interpretation of the references to color in this figure legend, the reader is referred to the web version of this article.)

either from Osetsky and Bacon [39] or from Terentyev et al. [28] were performed with different EAM interatomic potential for α-Fe and with different stress control fixed by a constant strain rate. The fact that similar results are found in the present study although the simulation techniques are different makes us confident in their robustness. The dislocation bypassing has been examined with different orientations of the habit plane for ⟨1 0 0⟩ loops, hereafter named $v1$ and $v2$. The former (chosen in Fig. 1(c)) leads to an attractive interaction whereas the interaction is repulsive with the latter.

Another point of interest is the characteristic shape of the dislocation at the CRSS. While it is very similar in the case of voids and

C15 clusters, with a well pronounced cusp which corresponds to the formation of a screw dipole behind the obstacle, in the case of ⟨1 0 0⟩ loops the angle between the two branches of the dislocation is fixed by the orientation of the loop itself and we notice the absence of screw dipole. In spite of these differences in the way the bypassing proceeds, the level of CRSS is only slightly modified as shown further. In the all three cases shown in Fig. 1, we notice the formation of vacancies at boundary of the obstacles (see insets).

The interactions between the dislocation and the SIA loops with 1/2⟨1 1 1⟩ Burgers vector differ from that with other clusters. We have noticed that after the procedure of energy relaxation the 1/2⟨1 1 1⟩ loops extend over several atomic planes thence yielding a faulted ribbon which forms a cylinder. This ribbon like form is a property inherent to the internal structure of SIA defects situated along the ⟨1 1 1⟩ directions. The most stable configuration of a single SIA situated along the ⟨1 1 1⟩ direction corresponds to the crowdion configuration in which the atoms along the ⟨1 1 1⟩ direction are slightly displaced from their equilibrium position. Those displacements decrease gradually from the center of mass of the defect to few nearest neighbor distance [40] along the ⟨1 1 1⟩ lines. The 1/2⟨1 1 1⟩ dislocation loops corresponds to a bunch of crowdions defects bonded by a very small attractive lateral crowdion–crowdion interaction [41], which preserves the two dimensional character of the dislocation loops. The ribbon like form comes from the relaxation of crowdions along the ⟨1 1 1⟩ direction which is larger for the defects located in the middle of the loop compared to those close to the border. Fig. 2(a) reproduces the typical result from our simulations (see inset (i) in Fig. 2(a)). The SIA that have been introduced in the perfect bcc lattice (the atoms colored in violet in Fig. 2(a)) are surrounded by a ribbon of fault, an assembly of atoms initially situated near the perfect lattice sites of the bcc lattice and which after energy relaxation have no longer the bcc symmetry in their first neighbor cells (atoms colored in red in Fig. 2(a) (i)). The formation of such a faulted ribbon can be viewed also as the consequence of the low migration energy barrier of these loops much like ⟨1 1 0⟩{1 1 1} dislocations in face centered cubic crystal that are well-known to have small Peierls barriers. We also notice that the habit planes of the 1/2⟨1 1 1⟩ loops rotate when these loops are situated in the vicinity of the edge dislocation. Such a rotation, also observed by different authors [42] is shown in Fig. 2(a) from insets (i, ii and iii). The SIA's that we have introduced (atoms colored in violet) and that initially determined the habit plane are eventually transferred into nearly perfect lattice sites, and at the end of relaxation procedure the orientation of the habit plane has changed to minimize the interaction energy with the dislocation.

According to our tests with quasi-static simulations, i.e. in absence of thermal effects, below a critical number of interstitial atoms, denoted by n_{sia} (we have determined that $8 < n_{sia} < 17$), the interaction with the dislocation is not sufficient to unpin the 1/2⟨1 1 1⟩ loop from the crystal lattice and the reaction between the dislocation and the loop is then similar to what have been described for the ⟨1 0 0⟩ loops (see Fig. 1(c)). Above n_{sia}, the interaction with the dislocation overpasses the loop migration barriers and the loops glide with the dislocation under the effect of the applied stress. This process is described in Fig. 2(b). Since with thermal effects the mobility of loops increases [43], it seems reasonable to think that increasing temperatures leads to a decrease of the critical number n_{sia} and that for high enough temperatures the loops of all sizes are dragged by edge dislocations. We can therefore expect that in iron based alloys where the edge dislocations propagate in the very first stage of the deformation tests (i.e. under small applied stresses) and vanish at the surfaces, the irradiation yielded 1/2⟨1 1 1⟩ loops should be dragged by edge dislocations toward surfaces. Hence, even though the formation of

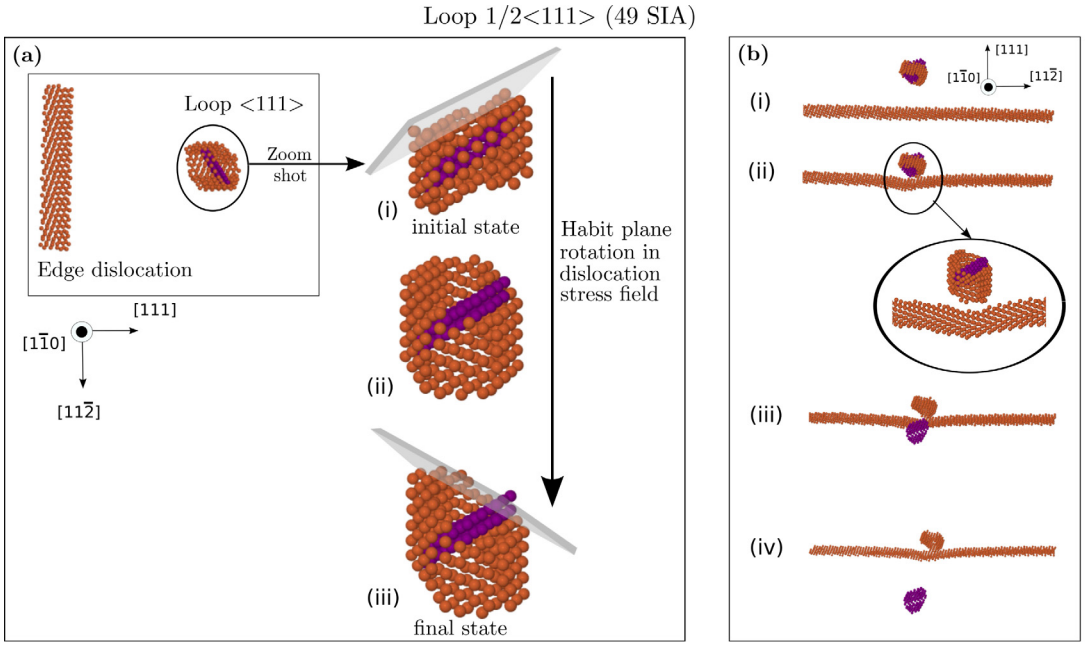

Fig. 2. (a) On the left-hand-side, simulation cell with an edge dislocation in interaction with a loop which Burgers vector is 1/2⟨1 1 1⟩. The color code is the same as in Fig. 1. The loop spreads spontaneously over few inter-atomic distances. Once placed in the stress field of the dislocation its habit plane rotates to achieve the minimal energy configuration (see text). Three stages of the rotation have been represented on the right-hand-side. The atoms colored in violet, initially SIA's become atoms of the perfect lattice in the course of the habit plane rotation. (b) Snapshots of edge dislocation glide in interaction with a 1/2⟨1 1 1⟩ loop made of 49 SIA's. The different stages of the simulations are represented: (i) initial configuration at a stress smaller than the Peierls stress (≈25 MPa), (ii) the dislocation glides toward the loop at a stress of the order of the dislocation Peierls stress, (iii) the loop becomes mobile at a sufficiently large stress, (iv) once the loop is depinned the dislocation and the loop glide all together. The atoms colored in violet mark the initial position of the loop. (For interpretation of the references to color in this figure legend, the reader is referred to the web version of this article.)

$1/2\langle 1\,1\,1\rangle$ loops could be a dominant process in the course of irradiation [44], along the very first stage of a deformation process the material could be swept up by the edge dislocations and only irradiation defects that are different from $1/2\langle 1\,1\,1\rangle$ loops could remain in majority.

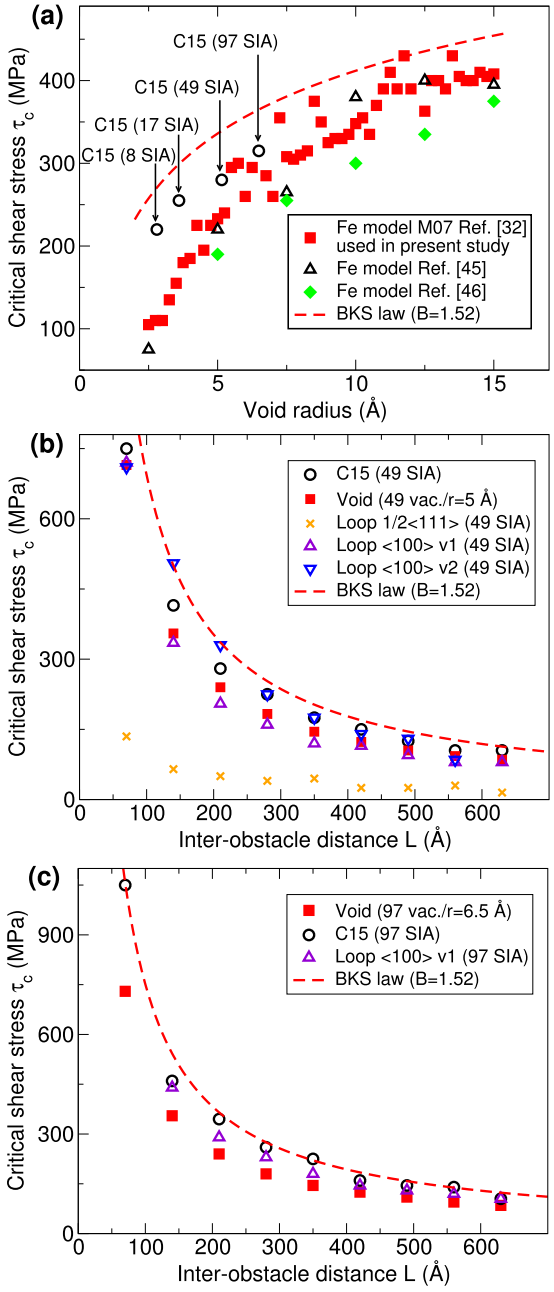

Fig. 3. (a) Critical resolved shear stress (CRSS) for the edge dislocation crossing a periodic row of nano-voids against void radius computed with different atomic-scale models. The inter-obstacle distance is $L = 21$ nm, i.e. the distance between the void and its first periodic images. For comparison, CRSS for crossing C15 made of different numbers of SIA (empty circles) have been reported at radii corresponding to the same numbers of vacancy (see text). (b) CRSS computed for different L and for different types of obstacles: C15 clusters, voids with 49 vacancies, $1/2\langle 1\,1\,1\rangle$ loops with 49 self-interstitial atoms (SIA's) and $\langle 1\,0\,0\rangle$ loops with 49 SIA's and different orientations of habit plan ($v1$ and $v2$). (c) Same as in (B) but for 97 vacancies in voids and 97 SIA's in C15 and $\langle 1\,0\,0\rangle$ loops. In the three graphics, the theoretical formula given by Eq. (1), with the single parameter $B = 1.52$, is plotted as a dashed line.

In Fig. 3(a), we have reported the CRSS computed from atomic-scale simulations for voids against the radius of the void. In order to show how our computations vary according to the inter-atomic potential model, we have repeated the same computations with different EAM's [45,46]. From the data reported in Fig. 1(a), one notices that the different models lead to comparable critical stresses for voids. However, the relative stability [6] of the different clusters is only described satisfactorily by the EAM used for the present work. In Fig. 3(a), we have also plotted the CRSS obtained for the C15 clusters with different sizes, i.e. different numbers of SIA. We have ascribed these values at the radius that corresponds to the void with same number of vacancies. Due to their spherical geometries, the radius of voids and C15 clusters are similar. We remark in Fig. 3(a) that the C15 clusters correspond to the largest CRSS, especially at small sizes. The difference in strength increases as the cluster size decreases and the C15 clusters become neatly the strongest obstacles below 17 SIA's. The dispersion of the data obtained for voids is related to the steps that may form at the surface of cavities when they are initially introduced in the simulation cell.

In Fig. 3(b and c) the CRSS for different types of obstacle has been computed in different configurations, i.e. varying the sizes of the clusters and the inter-obstacle distances, i.e. the dimension of the simulation cell in X direction. In the same graphic, we report our results for the different types of cluster as a function of the number of elementary defects involved into their formations. The number of such elementary defects is denoted by n_d and it may represent a number of vacancy in the case of voids or a number of SIA in the cases of loops and C15 clusters. Once again we remark in both graphics Fig. 3(b and c) that the C15 clusters are amongst the strongest obstacles along with the loops which Burgers vector is $\langle 1\,0\,0\rangle$. However, the pinning strength of these loops varies with the orientation of the habit plane. It has been found that one orientation of $\langle 1\,0\,0\rangle$ loops corresponds to a pinning force smaller than C15 whereas another one has been predicted to be stronger. A thorough study of the micro-structure evolution, accounting for the formation energies would be required to determine the respective densities (i.e. the average inter-obstacle distances) and sizes of clusters in realistic conditions. The relative stability of C15 clusters [6] at small sizes, associated with the present results about their pinning strength allows us to think that these obstacles may play an important role in the plastic deformation of irradiated iron based alloys.

In Fig. 3(b), we have reported additionally the applied shear stress required to make the dislocation gliding with a loop which Burgers vector is $1/2\langle 1\,1\,1\rangle$ (see Fig. 2). It appears clearly that the CRSS is much smaller than for other types of cluster which supports our belief that the contribution of these loops to the material hardening can be neglected. For inter-obstacle distances larger than 400 Å, the CRSS becomes comparable to the dislocation Peierls stress whereas it is found larger than 100 MPa for other clusters. Our conclusion is that the irradiation induced hardening of bcc iron based alloys would be mainly due to the formation of other types of cluster.

3. Theoretical analysis of atomic simulations

The comparison of the predictions based on BKS theory for voids hardening Eq. (1) with atomic-scale computations is presented against the nano-void radius r in Fig. 3(a) and against the inter-voids distance L in Fig. 3(b), where we have reported the theoretical predictions as dashed lines. The effective modulus G is defined by a formula established by Scattergood and Bacon [19]: $G = E_s/4\pi b^2$ where E_s corresponds to the pre-logarithmic part of the screw dislocation energy. We have chosen $G = 62.5$ GPa as

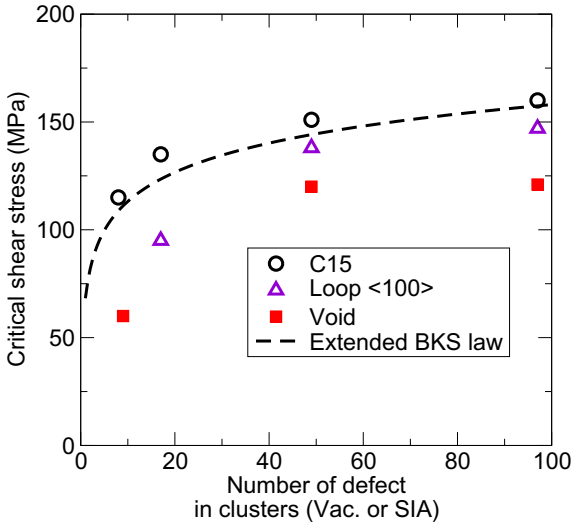

Fig. 4. Critical shear stress computed from simulations (symbols) against the number of elementary defect involved into the different clusters: voids, C15 clusters and ⟨1 0 0⟩ loops with *v*1 orientation. The inter-obstacle distance is $L = 420$ Å. The dashed line corresponds to the predictions from Eq. (2) with a coefficient $C = 4.0$.

earlier determined for the same system by different authors [23,25]. In a very same manner [23], the B parameter is fixed to $B = 1.52$ provided that r and L are expressed in unit of b in the logarithmic term of Eq. (1). In our simulation cells, $L \gg r$ such that the distance L can be considered as equal to the simulation cell dimension along X direction. It is remarkable that the parameters in Eq. (1) have not been adjusted to fit the simulation data reported in Fig. 3(a–c) and that nevertheless the theory provides same trends as simulations with a rather good qualitative agreement. The theory deviates from simulation data for small cavities, i.e., r below 5 Å, which is not surprising since the BKS formalism was derived for obstacles larger than 10 nm [19,23].

In Fig. 3(a–c), the BKS theory is in rather good agreement with the CRSS computed from simulations for C15 clusters and ⟨1 0 0⟩ loops. To the degree of approximation of the theory, we can consider that the very same theory predicts well the pinning strength for C15 clusters as well as for ⟨1 0 0⟩ loops provided that we consider clusters with a number of SIA equal to the number of vacancy involved into voids. The reason for such a correlation remains unexplained theoretically. On the basis of our simulations we can nevertheless generalize BKS theory to obstacles as C15 clusters and dislocation loops with ⟨1 0 0⟩ Burgers vector. In Eq. (1), we substitute r using the dimensional argument $r^3 \propto n_d$ which is valid for voids since their geometry is spherical above a certain radii. In the case of large inter-obstacle distances, $r \ll L$ the generalized BKS theory writes as follows:

$$\tau_{BKS} = \frac{Gb}{6\pi L}[\ln(n_d) + C]. \qquad (2)$$

where C is a coefficient which is related to B in Eq. (1).

The predictions obtained through Eq. (2) have been reported in Fig. 4 where they can be compared to the simulation data for different clusters with different numbers of elementary defects n_d. It clearly appears for all clusters that Eq. (2) gives the order of magnitude and the correct trend for the critical resolved shear stresses associated to every type of cluster, with only one adjusted parameter, namely C.

4. Conclusion

Employing an atomic-scale model for α-Fe, the depinning of an edge dislocation has been studied in simulations where a regular array of equidistant nano-obstacles was placed across the slip system. In agreement with earlier studies where different theoretical tools were used [15,19,39], the pinning of dislocation by nano-voids has been recognized as stronger than the process of Orowan loop formation which occurs when the dislocation encounters impenetrable obstacles.

The pinning strength computation has been extended to other types of irradiation defect including the C15 clusters and the loops with either ⟨1 0 0⟩ or ⟨1 1 1⟩ Burgers vector. According to the present simulations, the C15 clusters correspond to pinning strengths larger than for other types of defect when the comparison is made between clusters involving the same number of elementary defects (i.e. SIA's for C15 clusters and ⟨1 0 0⟩ loops and vacancies for voids). The difference in strength increases as the cluster size decreases and the C15 clusters become neatly the strongest obstacles below 17 SIA, i.e. at dimensions that are hardly visible with current experimental observation tools. At that sizes the C15 clusters are energetically the most stable interstitial defects in iron [6,7]. The present work can be viewed as preliminary to the determination of the role of C15 in hardening by irradiation in Fe alloys, which requires the proper determination of the different cluster densities and typical sizes. However, we have also shown that above 17 SIA, the C15 clusters and ⟨1 0 0⟩ loops correspond to pinning strengths similar to those for voids with same number of elementary defects. In this range of sizes where the different clusters have similar pinning strengths we have shown that the BKS theory could be applied to determine hardening with no adjustable parameter. The BKS law has been extended to C15 clusters and ⟨1 0 0⟩ loops (see Eq. (2)). The analytic theory has been found to correlate well with atomic scale computations for the pinning strength of voids, C15 clusters and ⟨1 0 0⟩ loops on the condition that we consider clusters with same numbers of SIA or vacancy. Although we admit that a serious theoretical grounding is missing, the practical interest of such a formula allowing us to estimate hardening for all types of cluster (excepted 1/2⟨1 1 1⟩ loops which the contribution can be neglected) opens promising possibilities for a multiscale treatment of irradiation hardening. Conversely, the interaction with dislocation loops which Burgers vector is 1/2⟨1 1 1⟩ impedes much less the dislocation mobility. We have shown that a moving edge dislocation could drag these loops in the glide direction under an applied shear stress much smaller than the CRSS obtained for other defects. Such a result allows us to expect that after the very first stage of deformation in iron based crystals, where no edge dislocation appears because of their high mobility and their swallowing at boundaries, the 1/2⟨1 1 1⟩ loops are cleaned up, possibly dragged to boundaries by the highly mobile edge dislocations. This sketch would provide the explanation for scarcity of 1/2⟨1 1 1⟩ loops in the experimental observations at low temperatures [47,48].

Acknowledgements

This work has been carried out within the framework of the EUROfusion Consortium and has received funding from the Euratom research and training program 2014–2018 under grant agreement No 633053. The views and opinions expressed herein do not necessarily reflect those of the European Commission. We acknowledge inspiring discussions with François Willaime.

References

[1] S. Dudarev et al., The EU programme for modelling radiation effects in fusion reactor materials: an overview of recent advances and future goals, J. Nucl. Mater. 386–388 (2009) 1.
[2] M. Lambrecht et al., On the correlation between irradiation-induced microstructural features and the hardening of reactor pressure vessel steels, J. Nucl. Mater. 406 (2010) 84.
[3] E. Gaganidze, H.-C. Schneider, B. Dafferner, J. Aktaa, Embrittlement behavior of neutron irradiated RAFM steels, J. Nucl. Mater. 367–370 (2007) 81.
[4] B.C. Masters, Dislocation loops in irradiated iron, Nature 200 (1963) 254.
[5] S.L. Dudarev, R. Bullough, P.M. Derlet, Effect of the α-γ phase transition on the stability of dislocation loops in bcc iron, Phys. Rev. Lett. 100 (2008) 135503.
[6] M.-C. Marinica, F. Willaime, J.-P. Crocombette, Irradiation-induced formation of nanocrystallites with *c*15 laves phase structure in bcc iron, Phys. Rev. Lett. 108 (2012) 025501.
[7] L. Dézerald, M.C. Marinica, L. Ventelon, D. Rodney, F. Willaime, Stability of self-interstitial clusters with c15 laves phase structure in iron, J. Nucl. Mater. 449 (2014) 219.
[8] J. Marian, B.D. Wirth, J.M. Perlado, Mechanism of formation and growth of ⟨1 0 0⟩ interstitial loops in ferritic materials, Phys. Rev. Lett. 88 (2002) 255507.
[9] H. Xu, R.E. Stoller, Y. Osetsky, D. Terentyev, Solving the puzzle of ⟨1 0 0⟩ interstitial loop formation in bcc iron, Phys. Rev. Lett. 110 (2013) 265503.
[10] Y. Zhang, X.-M. Bai, M.R. Tonks, S.B. Biner, Formation of prismatic loops from c15 laves phase interstitial clusters in body-centered cubic iron, Scr. Mater. 98 (2015) 5.
[11] I. Robertson, C. English, M. Jenkins, Low dose neutron-irradiation damage in α-iron, J. Nucl. Mater. 108–109 (1982) 209.
[12] S.J. Zinkle, B.N. Singh, Microstructure of neutron-irradiated iron before and after tensile deformation, J. Nucl. Mater. 351 (2006) 269–284.
[13] A.C. Nicol, M.L. Jenkins, M.A. Kirk, Matrix damage in iron, in: Symposium R – Microstructural Processes in Irradiated Materials-2000, volume 650 of MRS Proceedings, 2000.
[14] A. Foreman, M. Makin, Dislocation movement through random arrays of obstacles, Philos. Mag. 14 (1966) 911.
[15] R. Scattergood, D. Bacon, The strengthening effect of voids, Acta Metall. 30 (1982) 1665.
[16] L. Kubin et al., Solid state phenomena, in: G. Martin, L.P. Kubin (Eds.), Nonlinear Phenomena in Materials Science II, volume 23 & 24, Sci-Tech, Vaduz, 1992, p. 455.
[17] V.V. Bulatov, W. Cai, Computer Simulation of Dislocations, Oxford University Press, New York, 2006.
[18] D.J. Bacon, U.F. Kocks, R.O. Scattergood, The effect of dislocation self-interaction on the Orowan stress, Philos. Mag. 28 (1973) 1241.
[19] R. Scattergood, D. Bacon, The Orowan mechanism in anisotropic crystals, Philos. Mag. 31 (1975) 179.
[20] M. Daw, M. Baskes, Semiempirical, quantum mechanical calculation of hydrogen embrittlement in metals, Phys. Rev. Lett. 50 (1983) 1285.
[21] D. Bacon, Y. Osetsky, D. Rodney, Dislocation-obstacle interactions at the atomic level, in: J. Hirth, L. Kubin (Eds.), Dislocations in Solids, vol. 15, Elsevier, Amsterdam, 2009, p. 1.
[22] E. Bitzek, D. Weygand, P. Gumbsch, Atomistic study of edge dislocations in fcc metals: drag and inertial effects, in: H. Kitagawa, Y. Shibutani (Eds.), Mesoscopic Dynamics of Fracture Process and Materials Strength, Kluwer Academic Publishers, Dordrecht, 2004, p. 45.
[23] Y. Osetsky, D. Bacon, Void and precipitate strengthening in α-iron: what can we learn from atomic-level modelling?, J Nucl. Mater. 323 (2003) 268.
[24] S.H. Haghighat, J. Fikar, R. Schäublin, Effect of interatomic potential on the behavior of dislocation-defect interaction simulation in α-fe, J. Nucl. Mater. 382 (2008) 147.
[25] R. Schäublin, S.H. Haghighat, Molecular dynamics study of strengthening by nanometric void and cr alloying in fe, J. Nucl. Mater. 442 (2013) S643.
[26] D. Wirth, V. Bulatov, T.D. de la Rubia, Dislocation-stacking fault tetrahedron interactions in Cu, J. Eng. Mater. Technol. 124 (2002) 329.
[27] D. Rodney, G. Martin, Dislocation pinning by glissile interstitial loops in a nickel crystal: a molecular-dynamics study, Phys. Rev. B 61 (2000) 8714.
[28] D. Terentyev, P. Grammatikopoulos, D. Bacon, Y.N. Osetsky, Simulation of the interaction between an edge dislocation and a 100 interstitial dislocation loop in α-iron, Acta Mater. 56 (2008) 5034.
[29] D. Terentyev, Y. Osetsky, D. Bacon, Competing processes in reactions between an edge dislocation and dislocation loops in a body-centred cubic metal, Scr. Mater. 62 (2010) 697.
[30] S. Queyreau, G. Monnet, B.D. Wirth, J. Marian, Modeling the dislocation-void interaction in a dislocation dynamics simulation, in: Symposium P - Deformation Mechanisms, Microstructure Evolution and Mechanical Properties of Nanoscale Materials, volume 1297 of MRS Proceedings, 2011, pp. 10–61.
[31] X.J. Shi, L. Dupuy, B. Devincre, D. Terentyev, L. Vincent, Interaction of ⟨1 0 0⟩ dislocation loops with dislocations studied by dislocation dynamics in α-iron, J. Nucl. Mater. 460 (2015) 37.
[32] L. Malerba et al., Comparison of empirical interatomic potentials for iron applied to radiation damage studies, J. Nucl. Mater. 406 (2010) 19.
[33] L. Proville, D. Rodney, M.-C. Marinica, Quantum effect on thermally activated glide of dislocations, Nat. Mater. 11 (2012) 845.
[34] B. Barvinschi, L. Proville, D. Rodney, Quantum peierls stress of straight and kinked dislocations and effect of non-glide stresses, Modell. Simul. Mater. Sci. Eng. 22 (2014) 025006.
[35] S. Patinet, L. Proville, Depinning transition for a screw dislocation in a model solid solution, Phys. Rev. B 78 (2008) 104109.
[36] D. Rodney, L. Proville, Stress-dependent peierls potential: Influence on kink-pair activation, Phys. Rev. B 79 (2009) 094108.
[37] L. Proville, B. Bakó, Dislocation depinning from ordered nanophases in a model fcc crystal: from cutting mechanism to Orowan looping, Acta Mater. 58 (2010) 5565.
[38] S.H. Haghighat, M. Fivel, J. Fikar, R. Schäublin, Dislocation-void interaction in fe: a comparison between molecular dynamics and dislocation dynamics, J. Nucl. Mater. 386–388 (2009) 102.
[39] D. Bacon, Y. Osetsky, The atomic-scale modeling of dislocation-obstacle interactions in irradiated metals, JOM 59 (2007) 40.
[40] S.P. Fitzgerald, D. Nguyen-Manh, Peierls potential for crowdions in the bcc transition metals, Phys. Rev. Lett. 101 (2008) 115504.
[41] P.M. Derlet, D. Nguyen-Manh, S.L. Dudarev, Multiscale modeling of crowdion and vacancy defects in body-centered-cubic transition metals, Phys. Rev. B 76 (2007) 054107.
[42] D. Terentyev, Public communication at IREMEV meeting in Garching, 2014.
[43] P.M. Derlet, M.R. Gilbert, S.L. Dudarev, Simulating dislocation loop internal dynamics and collective diffusion using stochastic differential equations, Phys. Rev. B 84 (2011) 134109.
[44] J. Marian, B.D. Wirth, J.M. Perlado, Mechanism of formation and growth of ⟨1 0 0⟩ interstitial loops in ferritic materials, Phys. Rev. Lett. 88 (2002) 255507.
[45] P. Gordon, T. Neeraj, M. Mendelev, Screw dislocation mobility in bcc metals: a refined potential description for α-fe, Philos. Mag. 91 (2011) 3931.
[46] H. Chamati, N. Papanicolaou, Y. Mishin, D. Papaconstantopoulos, Embedded-atom potential for fe and its application to self-diffusion on fe (1 0 0), Surf. Sci. 600 (2006) 1793.
[47] E. Meslin, A. Barbu, L. Boulanger, B. Radiguet, P. Pareige, K. Arakawa, C. Fu, Cluster-dynamics modelling of defects in α-iron under cascade damage conditions, J. Nucl. Mater. 382 (2008) 190.
[48] D. Brimbal, B. Décamps, A. Barbuc, E. Meslin, J. Henry, Dual-beam irradiation of α-iron: heterogeneous bubble formation on dislocation loops, J. Nucl. Mater. 418 (2011) 313.